PCCP

ARTICLE TYPE

Cite this: DOI: 00.0000/xxxxxxxxxx

Insight in the Role of Excess Hydroxide ion in Silicate Condensation Reaction

Tuong Ha Do,[a], Hien Duy Tong,[b], Khanh-Quang Tran,[c] Evert Jan Meijer,*[d] and Thuat T. Trinh *[e]

Received Date
Accepted Date

DOI: 00.0000/xxxxxxxxxx

The formation of silicate oligomers in the early stages is key to zeolite synthesis. The pH and the presence hydroxide ions are important in regulating the reaction rate and the dominant species in solutions. This paper describes the formation of dimer to 4-ring silicate species using *ab-initio* molecular dynamics simulation in explicit water molecules with an excess hydroxide ion. The thermodynamic integration method was used to calculate the free energy profile of the condensation reactions. The hydroxide group's role is not only to control the pH of the environment, but also to actively participate in the condensation reaction. The results show that the most favorable reactions are linear tetramer and 4-ring formation, with overall barriers of 71 kJ/mol and 73 kJ/mol, respectively. The formation of trimer silicate with the largest free energy barrier of 102 kJ/mol is the rate-limiting step in this condition. The excess hydroxide ion aids in the stabilization of the 4-ring structure over the 3-ring structure. Due to a relatively high free energy barrier, the 4-ring is the most difficult of the small silicate structures to dissolve in the backward reaction. This study is consistent with the experimental observation that silicate growth in zeolite synthesis is slower in a very high pH environment.

1 Introduction

Zeolites are nanoporous aluminosilicate materials widely used in various industrial applications making use of their catalytic and separation properties[1]. Zeolites are typically synthesized from aqueous gel solutions containing various heteroatomic compounds, with inorganic and/or organic cations acting as directing agents of the structures. Numerous experimental[2–10] studies have focused on the nature and structure of the silicate oligomers in solution, as understanding the formation of silicate oligomers in the initial stage is key to zeolite synthesis[11,12]. The initial steps for silicate oligomerization were also extensively studied in computational studies using a continuum[13–23] or explicit model[11,24–27] of water. A common pathway of the oligomerization reaction is a two-step mechanism with an initial formation of a penta-coordinated intermediate, followed by a water removal stage[24,25,28–32]. Earlier studies (e.g. Refs[24?,25]) have shown that it is crucial to include the effect of thermal motion and the presence of explicit water molecules, when modeling aqueous chemical reactions that involve solvent molecules that strongly bind to the reagents, or actively participate in the reaction mechanism. The overall picture of free energy profiles and mechanism could change significantly with dynamic and explicit treatment of solvent. Ions have an important role in the silicate condensation reaction. For example, organic cations (such as tetramethylamine (TMA^+), tetraethylamine (TEA^+), tetrapropyl amine(TPA^+)) were shown to have a decisive role in the formation of dominating silicate spices during the initial state of zeolite formation[33,34]. Computational studies indicated that inorganic cations (such as Li^+, Na^+, $NH_4{}^+$) also have a substantial impact on the activation barrier of the condensation reaction[25,28]. Furthermore, pH is recognized as one of the most important parameters for controlling the kinetic and structural aspects of silicate oligomerization. Neither an extremely high nor an extremely low pH is required for silicate oligomerization to occur at its fastest rate[35]. According to experiments, the silicate oligomerization rate is maximal at pH ≈ 8[36,37]. The first acid dissociation constant of silicic acid at 298 K is $pK_{a1} = 9.84$[38]. At basic conditions,

[a] *Faculty of Applied Sciences, Ton Duc Thang University, 19 Nguyen Huu Tho, Tan Phong ward, District 7, Ho Chi Minh City, Vietnam, E-mail:dotuongha@tdtu.edu.vn*
[b] *Faculty of Engineering, Vietnamese-German University (VGU), Thu Dau Mot City, Binh Duong Province, Vietnam*
[c] *Department of Energy and Process Engineering, Norwegian University of Science and Technology, Kolbjørn Hejes vei 1B, Trondheim, Norway*
[b] *Van't Hoff Institute for Molecular Sciences, University of Amsterdam, Amsterdam, The Netherlands*
[d] *Department of Chemistry, Norwegian University of Science and Technology, Høgskoleringen 5, 7491-Trondheim, Norway*
* *E-mail:e.j.meijer@uva.nl, thuat.trinh@ntnu.no*
† Electronic Supplementary Information (ESI) available: [More details on the thermodynamic integration, radial distribution of water, molecular orbital and selected bond lengths and angles are provided]. See DOI: 10.1039/cXCP00000x/

the equilibrium between silicic acid $Si(OH)_4$ and its deprotonated form $Si(OH)_3O^-$ is given by 1:

$$Si(OH)_4 + OH^- = Si(OH)_3O^- + H_2O \quad (1)$$

After the deprotonation step of silicic acid, the first silicate condensation reaction proceeds via 2:

$$Si(OH)_4 + Si(OH)_3O^- = Si_2O_7H_5^- + H_2O \quad (2)$$

However, in the presence of an excess of hydroxide ions, an alternative pathway involving two negatively charged silicate monomers is possible via 3:

$$Si(OH)_3O^- + Si(OH)_3O^- = Si_2O_7H_4^{2-} + H_2O \quad (3)$$

Previous studies[29,39] mostly neglecting pathway 3 and accounted for the role of hydroxide ions via the ratio between the $Si(OH)_4$ and $Si(OH)_3$ in equilibrium. This simplification captures the microkinetic model of the condensation process and assumes that the presence of OH^- has no effect on the condensation reaction's reaction barrier[29]. Understanding the pH effects of the presence of anions in solution is an important area of research. For example, Biswas et al.[40,41] utilized metadynamics simulations to study the deprotonation process of organic ions in various solvents. Their findings shed light on the influence of solvent composition on the deprotonation reaction and highlighted the role of solvent dynamics in the proton transfer mechanism. However, there has been little research into how OH^- interacts with reactive species during silicate oligomerization.

In this work, *ab-initio* molecular dynamic (AIMD) simulations were performed to study the formation of silicate oligomers in the presence of an excess OH^- ion in aqueous solution, incorporating the water molecules explicitly. The free energy profiles of the reaction pathways to different silicate oligomers, from dimer up to 4-ring species, were obtained. Details of the pathways and associated free energy profiles will be discussed. We will provide evidence for an active role of the OH^- ion in the condensation reaction, and will show that the rate-limiting step of the process is the formation of the trimer structure. This might explain why the silicate condensation reaction is not favorable at very high pH, as observed in the experiment.

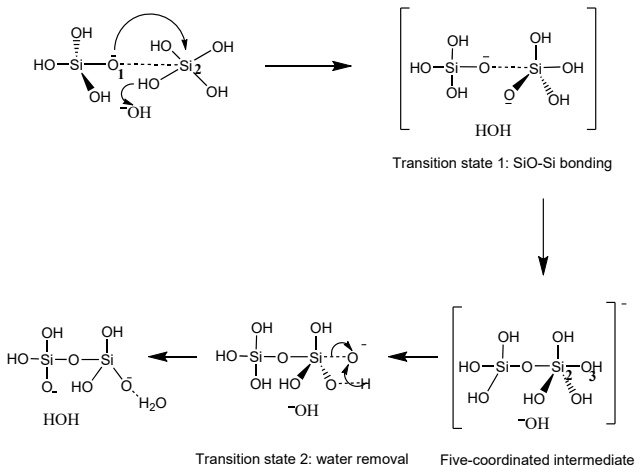

Scheme 1 Representation of a two-step mechanism of silicate condensation reaction with the presence of excess OH^-. R, TS1, I, TS2, P refers to reactant, transition state 1, intermediate, transition state 2, and product, respectively.

2 Simulation Method

Our computational setup was similar to that of earlier computational studies of silicate oligomerization reactions in aqueous solution[24,25,28]. The *ab-initio* molecular dynamic simulations are based on a density functional theory (DFT) description of the electronic structure. We employed the CP2K package[42] to carry out the molecular dynamics simulation using a Born-Oppenheimer approach as implemented in the Quickstep module[43]. Here, Goedecker-Teter-Hutter (GTH) pseudopotentials[44,45] are used to account for the interactions between the electrons and the atomic nuclei. The BLYP exchange-correlation functional[46,47] was used, complemented with Grimme's D2[48] correction, to account for the long range van der Waals interactions. A double-zeta valence basis set complemented with polarization functions[49] (DZVP-MOLOPT) was employed for all atom types. An energy cut-off of 400 Ry was chosen for the auxiliary plane wave basis set. The molecular dynamics trajectories were generate with a time step of 0.5 fs. We applied a canonical velocity re-scaling thermostat[50] with a time constant of 300 fs to impose the temperature of the system. The temperature was set at 350 K, which is consistent with the experimental conditions used for zeolite synthesis in solution[35,51]. This temperature is also frequently used in molecular simulations for this type of system[29,30,52].

The simulation cell was a periodic orthorhombic box (around 16x16x16 $Å^3$). The dimension of the simulation box was adjusted in each system to have a density of 1 g/cm^3, similar to that of the experimental value[35,51]. The initial geometry of the silicate reactants and a hydroxide ion OH^- was first optimized in the gas phase. This structure was then solvated with around 128 water molecules evenly distributed in the simulation box. Subsequently, to generate a representative configuration, a 20 ps equilibration run was performed in the NVT ensemble. The total number of atoms in the system was approximately 420 atoms. Due to the high computational cost inherent to *ab-initio* MD, we did not consider with systems of larger size or a higher concentration of silicate in the present study.

Reaction pathways and associated free energy profiles were traced by imposing a set of values of a proper reaction coordinate using the method of constraints.[53,54] For each value of the reaction coordinate, the initial configuration was taken from the last configuration of the simulation at the previous value of the reaction coordinate. After 1 ps of equilibration run, a 10 ps trajectory of production run was generated. The total trajectory of the simulations of a reaction pathway was around 200 ps, distributed typically over 20 values of the reaction coordinate.

The free energy (ΔG) profiles of the oligomerization reactions

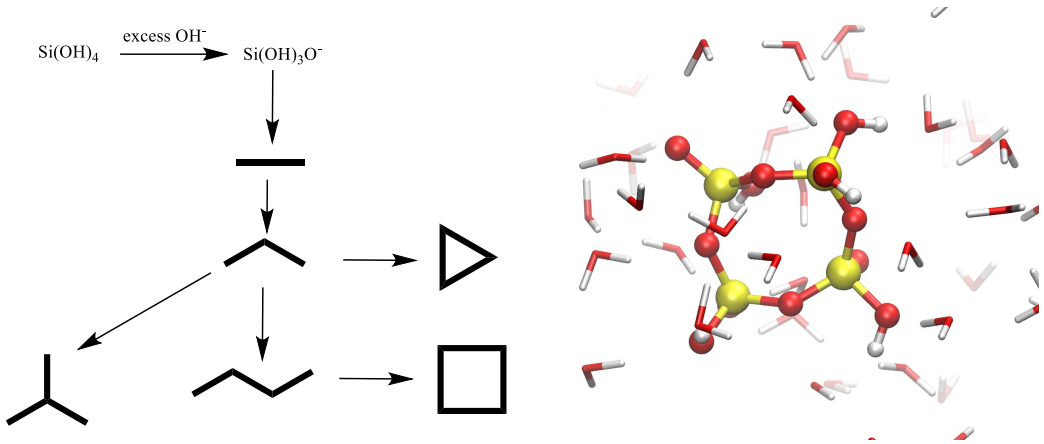

Fig. 1 Left: scheme of the oligomerization reactions considered in this work forming from dimer to 4-ring formation. Right: snapshot of *ab-initio* MD simulations for 4-ring formation. The system consists of silicate reactants, a OH^-, and 128 water molecules.

were obtained by thermodynamic integration using eq.4

$$\Delta G = \int_{r_1}^{r_2} \langle F(r) \rangle \, dr \tag{4}$$

Here, r denotes the reaction coordinate, and F is the calculated constraint force and r at a fixed value of the reaction coordinate. As illustrated in Scheme 1, the reaction coordinate r is typically the bonding distance between O_1-Si_2 and Si_2-O_3 for the first and the second steps of silicate condensation reaction, respectively. The value r_1 denoted for the reactant state and r_2 is for the product state. The values of r_1 and r_2 are the average distances determined by unconstrained AIMD of the system at those state. An example of the r values and forces for dimerization and trimerization reactions are provided in the Table S1 and Fig S1 of the Supporting Information. The integral is evaluated numerically on basis of the calculated values of the constraint force at each of the (∼20) reaction coordinate values. The errors of the constraint force are typically below 10^{-5} Hartree/Bohr in 10 ps production run. This approach has generic applicability, and is extensively in earlier studies to calculate free energy barrier reactions in solution[24,55–58] and oxidation of methane in solid state[59].

A common two-step mechanism of silicate condensation reaction in the basic conditions[28] is described in Scheme 1. The first step is Si-O bond formation, yielding an intermediate with a five fold coordinated Si. For this stage of the reaction pathway, the distance between atom O_3 and Si_2 was taken as reaction coordinate ($d1_{Si\text{-}O}$). Here, O_3 atom is defined as the reactive oxygen. The second stage consists of a water removal step, where the distance between Si_2 and O_4 was taken as the reaction coordinate ($d2_{Si\text{-}O}$). For ring closure reactions, a similar mechanism has been considered[28,52]. Note that in the ring closure reaction the silicon and oxygen atom in the first reaction step are of the same oligomer molecule. We investigated six oligomerization reactions, from the formation of a dimer up to a 4-ring structures. A schematic process of the reactions is provided in Fig. 1. For each of the systems one of the silica species was deprotonated. One extra hydroxide group was added into the system for each reaction, which leads to the doubly charged system in all cases. Positive background charge was automatically imposed by CP2K to balance the system's negative charge.[42].

3 Results and discussion

3.1 Structure of liquid phase

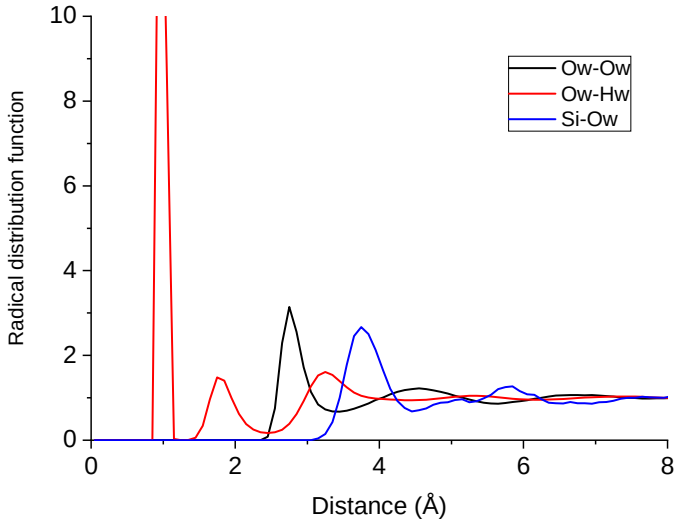

Fig. 2 Radial distribution function (RDF) for Ow-Ow, Ow-Hw, Si-Ow of silicate solvated in water, as obtained by unconstrained AIMD simulations.

The radial distribution function (RDF) is a key descriptor in the study of water structure and has been extensively investigated in the literature using various simulation[60–63] and experimental techniques[64–66]. In order to compare and validate our simulation approach, we performed AIMD simulations of pure water and computed the RDFs of Ow-Ow and Ow-Hw. The comparison of our AIMD using BLYP-D2 functional with the SCAN functional[63] and experimental results[65,66] is presented in Fig S2. The results show that our AIMD approach is in excellent agreement with both the SCAN functional and experimental data for the RDFs of Ow-Ow and Ow-Hw. These findings support the validity of our computational setup for studying silicate condensation reaction in wa-

ter.

To assess the effect of OH^- on the local structure of the system, we performed an unconstrained 20 ps AIMD simulation of the OH^- – deprotonated silicate monomer system. We quantified basic structural information of the system by RDFs of the water and silicate species. The RDFs of oxygen-oxygen (Ow-Ow) and oxygen-hydrogen (Ow-Hw) among water molecules, and silicon-water oxygen (Si-Ow) are shown in Fig. 2. For the Ow-Ow RDF the first peak is located at 2.8 Å, which is in good agreement with the experimental data and earlier simulations[52,63]. This confirms that the presence of OH^- and silicate has minor effect on the overall water structure. The first peak of Si-Ow RDF is located at 3.75 Å, which is very similar to the case without hydroxide anion[52].

To further assess the effect of the OH^- presence, we performed simulations with one deprotonated silica species. We considered two systems (see Fig. 3). The first system consists of 2 monomers, $Si(OH)_4$ and $Si(OH)_3O^-$, and one (excess) OH^- in aqueous solution. The initial position of OH- was created at random near one monomer $Si(OH)_4$. A aqueous hydroxide deprotonates the neutral silicate monomer in the first picosecond of the 20 ps trajectory, yielding one water molecule and a second negatively charged deprotonated silica species. (see Fig. 3.a). This demonstrates that, for the given system size, the excess OH^- induces a stable solvation of two negatively charged silicate monomers. As hydroxide is a stronger base than a silicate monomer (silicic acid has pK_{a1} of 9.84[38]), a deprotonation of the neutral silica species is to be expected. Note, that the deprotonation occured on a short time scale, within the first ps.

The second system addresses the presence of an excess OH in product state of a dimerization, i.e. a singly deprotonated silica dimer. Again an unconstrained simulation was performed with the excess hydroxide ion fully solvated by water molecules, but in the neighbourhood of the silicate dimer $Si_2O_7H_5^-$. As can be seen in Fig. 3.b, an a hydroxide almost immediatly deprotonates the silica dimer. The silicate species $Si_2O_7H_4^{2-}$ remains in the doubly deprotonated state during the subsequent 20ps of simulation. Fig. 3.b quantifies the deprotation step. It shows the distance of O_2-H_1 indicating that the silanol group transfers one H^+ to the hydroxide group, yielding a water molecule. While the change of the distance O_1-H_1 shows that the transferred proton is located in a water molecule far from the silicate at the end of simulation. Thus, the results confirm that excess hydroxide ion deprotonates spontaneously the silanol group of silicate dimer in both reactant and product state.

3.2 Formation of linear silicate oligomers

Fig. 4 presents representative snapshots of the silicate dimerization reaction with an excess hydroxide group. The reaction mechanism of silicate condensation is very similar to what is reported in earlier studies[28,30,67]. As described in Scheme 1, the first reaction step is to form SiO-Si bond resulting in 5-fold silicate intermediate. The second step is the removal of the water to form the dimer product. The trajectory shows interesting structural changes. In the reactant state, there are two anionic silicate $Si(OH)_3O^-$ surrounded by water network as described in the previous section. The distance between SiO–Si at the reactant state is located at 3.7 Å as shown in Fig. 4. This distance is shorter when the two silicate species approaches each other. At 2.2 Å, the location of the first transition state (TS1), we observe a proton transfer between the monomers. The structure at TS1 then appears as one neutral monomer and one doubly charged monomer (see Fig. 4). The reaction step produces a 5-fold intermediate silicate that is doubly charged. The second step of the reaction, water removal, is similar to what has previously been reported[52,68]. The second transition state (TS2), involves a leaving hydroxide group. The generated trajectory of this stage, showed an internal proton transfer from the intermediate state to the leaving hydroxide group, resulting in the formation of a water molecule. It's worth noting that the silicate species remains doubly deprotonated the dimerization pathway: intermediate, TS2, and product state.

The calculated free energies of various structures along the dimerization reaction are listed in Table 1. Taking the reactant state as the reference, the free energy barrier of the first reaction is 71 kJ/mol. The second activation barrier, calculated as the free energy difference between the transition state TS2 and the intermediate, is 24 kJ/mol. The resulting overall activation barrier of the dimer formation is 83 kJ/mol. This is an endothermic reaction with the free energy of reaction, calculated as the difference in free energy of the product and the reagents, is equal to 16 kJ/mol. This value is consistent with previous simulation of silicate condensation reaction in solution[24,52]. The presence of positively charged counter ions is known to increase the overall reaction barrier[25,67] due to the interaction between the cation and the hydrogen bonding network or the cation ion could interact directly with the reaction center. It is interesting to note that the same trend was observed in the present study, where there is an anionic environment. However, in this case, the increasing activation barrier is appear to be due to electrostatic interaction between negatively charged silicates. This raises the free energy barrier, and implies that the presence of neither a positive ion nor a negative anion does lower the activation barrier of the silicate (dimer) condensation reaction.

Table 1 also shows the free energy data for the formation of larger linear oligomers, i.e. the trimer and linear tetramer. The first step's energy barrier was highest in trimer formation and lowest in linear tetramer formation. As a result, the total energy barrier for trimerization is the highest, with an overall barrier of 102 kJ/mol, while the barriers for dimer and linear tetramer formation are only 83 kJ/mol and 71 kJ/mol, respectively. In contrast, without excess hydroxide ion, the dimerization reaction has a higher overall barrier than trimerization (see Table 2). It is not surprising that the second step free energy barriers for the formation of dimer, trimer, and linear tetramer are around 20-30 kJ/mol. These values are comparable to those observed in simulations of systems containing other cations[25,28]. In all cases, the hydroxide group that is leaving is embedded in a well-defined hydrogen bonds network with water molecules. It is protonated either directly by another silicate hydroxide group or indirectly through a proton transfer chain mediated by one or more water molecules. This is in consistent with previous studies showing

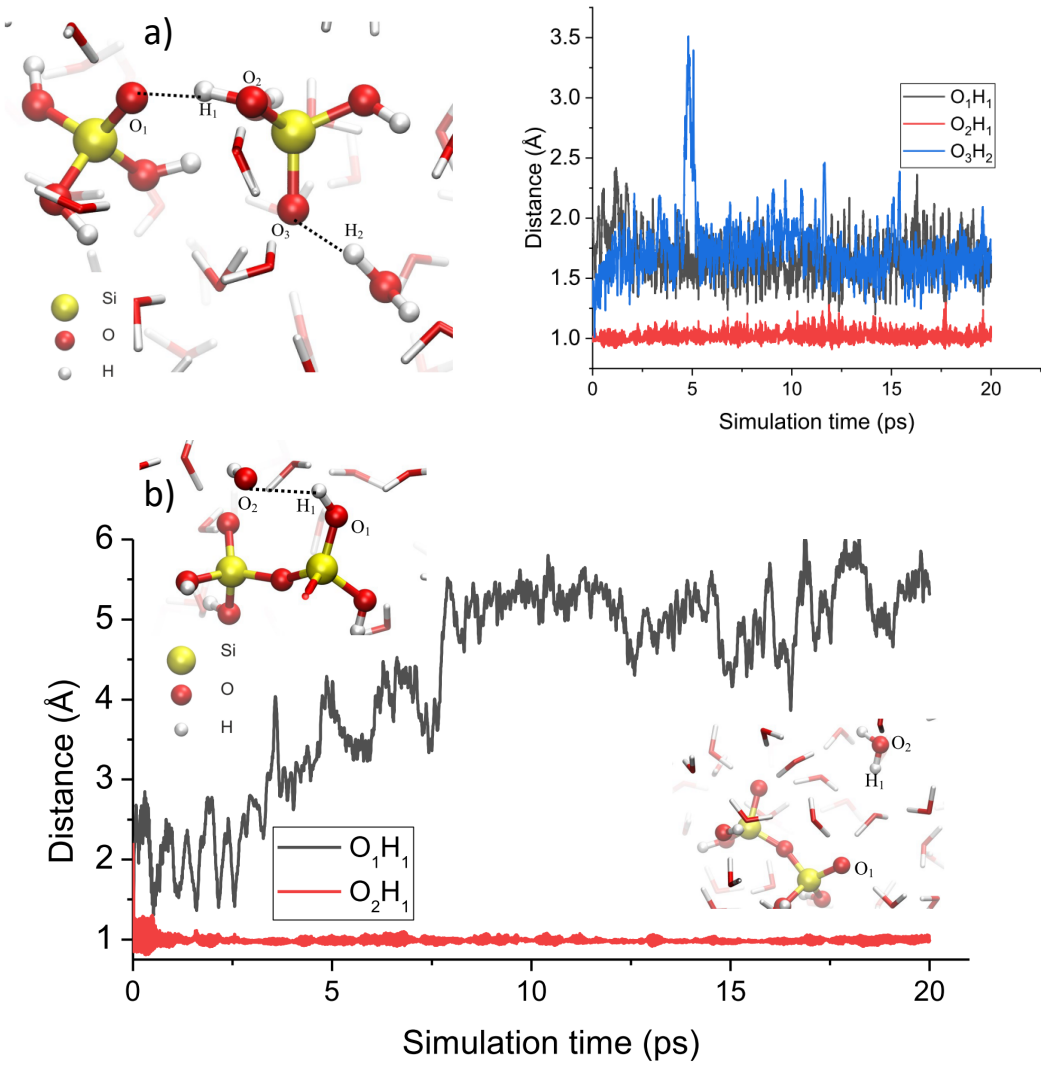

Fig. 3 Representative snapshot from the unconstrained AIMD simulations of silicate with the excess of hydroxide ion surrounding by water molecules. On the top (a), there is a proton transfer process for $Si(OH)_4 + Si(OH)_3O^- + OH^- \longrightarrow 2Si(OH)_3O^- + H_2O$. At the bottom (b), the trajectory shows proton transfer for dimer $Si_2O_7H_5^- + OH^- \longrightarrow Si_2O_7H_4^{2-} + H_2O$. The distance of selected oxygen-hydrogen bonding were presented during 20 ps of simulation time.

that this step is mostly determined by the aqueous solvation and associated hydrogen bonding network between silicate and water[68].

When we examined the free energy profile of the trimerization in greater detail, we noted that the first activation barrier is 10 kJ/mol higher than that of the dimerization. The second activation barrier of the water removal step, on the other hand, is more unfavorable (33 kJ/mol), whereas dimerization only has (24 kJ/mol). The free energy profiles of linear growth shown in Fig. 5 show that trimer formation has the highest energy in the TS1, intermediate, TS2, and product states. The linear tetramer formation has the lowest TS1, intermediate, and TS2 states. However, the dimerization product state is the most stable of the three. The overall picture suggests that the trimerization reaction is the rate-limiting step in formation of small silica oligomers. The observation that reaction-free energies are positive in this work complies with previous theoretical studies[25,30,68]. The reason is that the overall reaction yields one extra molecule of water which generates an entropically unfavorable rearrangement of the structure of water.

3.3 Formation of ring and branched silicate oligomers

One of the critical steps in zeolite growth is the formation of branched and ring structures. The formation of initial 3-ring or 4-ring structures, in particular, is a prerequisite for the formation of higher ring species of zeolites, such as double 3-ring (D3R) and double 4-ring (D4R). The mechanism of 3-ring and 4-ring configuration formation is comparable to that seen in simulations of linear structure formation. Earlier computational studies elucidated the details of this ring closure reaction.[28,52]. Fig. 6 shows representative snapshots of the 3-ring reaction pathway in the presence of excess hydroxide. The reactant state of the 3-ring formation is the linear trimer product with doubly charged state. The separa-

Table 1 Calculated free energy (kJ/mol) profiles along the silicate formation in the presence of excess hydroxide ion obtained by AIMD. All values are relative to the reactant state.

Free energy	reactant	TS1	intermediate	TS2	product
Dimer	0	71	59	83	16
Trimer	0	81	69	102	45
Linear Tetramer	0	61	41	71	24
3-ring	0	81	70	92	48
4-ring	0	60	45	73	7
Branched Tetramer	0	68	58	86	33

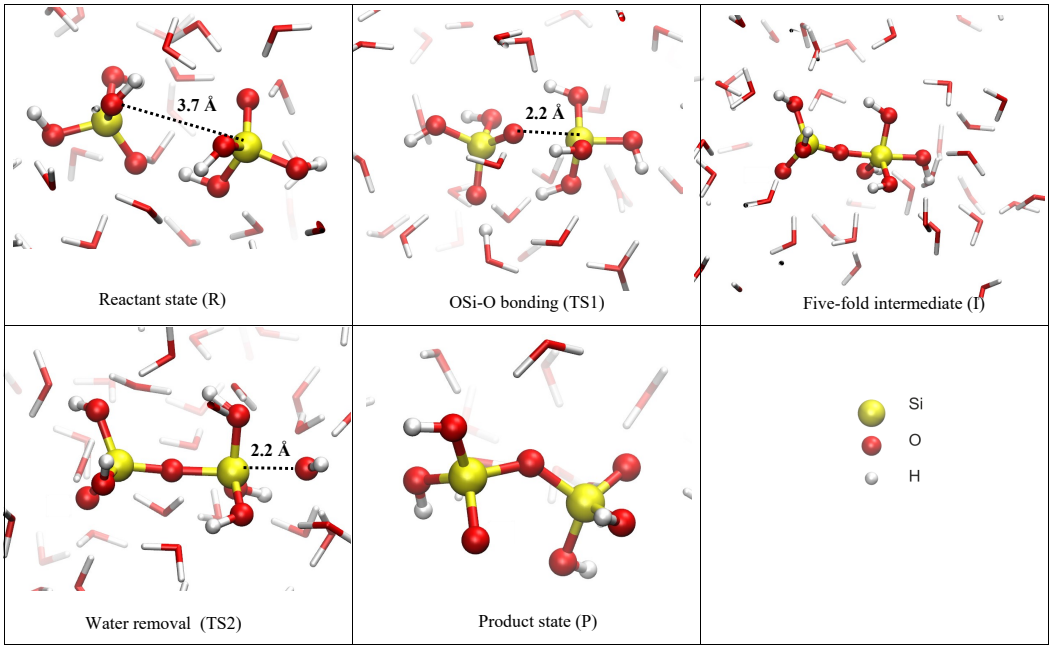

Fig. 4 Representative snapshot from AIMD simulations of the dimerization reaction with the excess of hydroxide ion. Reaction mechanism is described in Scheme 1. For clarity, some water molecules are omitted in the visualization.

Table 2 Total free energy barriers (kJ/mol) obtained by AIMD of silicate oligomerization reaction with presence of excess hydroxide ion. The free energies without excess hydroxide[27] is added for comparison.

Free energy barrier	with excess OH^- (this work)	without excess OH^- ref[27]
Dimer	83	61
Trimer	102	53
Linear Tetramer	71	/
3-ring	92	72
4-ring	73	95
Branched Tetramer	86	101

tion between active oxygen and silicon was at 3.7Å. The negative charge is distributed over two silicon atoms rather than one during the equilibrium run of the reactant state. An intermediate ring is formed when the active oxygen atom from one end of the linear trimer binds to the Si atom from the other end. We also noticed an internal proton transfer between two silanol groups. This proton transfer did, in fact, aid in the contact between the reactive oxygen and the Si atom in order to form the SiO-Si bond. The final product is produced in the second step, which involves the removal of water. The TS2's reaction coordinate is comparable to that of the TS1, both values are at 2.2 Å (see Fig. 6). It's worth noting that the leaving hydroxide group is protonated via an external transfer mechanism, which receives the proton from another water in the proximity. We observed that proton transfer between the silicate and water environments happens instantly throughout the reaction. At the same time, another proton transfers spontaneously from the silanol group to the water's hydrogen bond network, resulting in a doubly charged product state.

The details of free energy profiles of the formation of 3-ring, 4-ring and branched tetramer are presented in Table 1. The constraint force profiles along the reaction pathways of formation of 3-ring and 4-ring structures are presented in Fig S1. The 3-ring formation had the highest overall barrier (92 kJ/mol), while the 4-ring formation had the lowest activation barrier (73 kJ/mol). This distinction could be related to double negative charge that has a stronger unfavorable effect for a smaller molecule. Higher oligomers, such as 4-ring and branched tetramers, have lower activation because they are more stabilized and have an enhanced hydrogen bonding with water. It's worth noting that in the presence of an excess of hydroxide, the formation of the 4-ring is more favorable than that of the 3-ring. In the absence of excess hydroxide (see Table 2), this is the opposite. The reason could

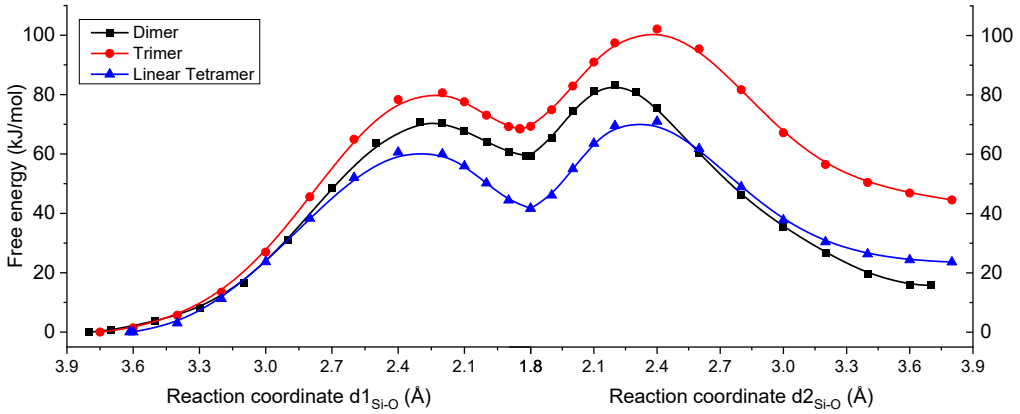

Fig. 5 Calculated free-energy profile (kJ/mol) of formation of linear silicate oligomers as a function of the reaction coordinate. The profiles calculated for the two stages are connected in the graph.

be that the charge distribution of the 4-ring varies with charged state. The stability of the 4-ring over the 3-ring has previously been observed when organic counter ion such as TMA^+ interacts with silicate.[52,69,70] Another ion such as TEA^+ shows the opposite trend[67]. In the presence of an excess hydroxide ion, the free energy profiles along the reaction process of 3-ring, 4-ring, and branched tetramer formation is shown in Fig. 7. We clearly see an increasing trend in the height of the free energy barriers, in the order 4-ring, branched tetramer, 3-ring. This indicates that in the presence of an excess of hydroxide, the formation of 3-ring structures is less likely, whereas the 4-ring structure and branched tetramer are more dominant in the early stages of silicate condensation.

The bonds and angles in the 3-ring and 4-ring structures were analyzed using AIMD simulations, and the resulting data were compared with previous DFT calculations[19] (Table S2). It should be noted that the DFT calculations were performed with static solvation using 16-18 water molecules around the silicate[19]. In contrast, our AIMD simulations were conducted with more than 128 water molecules, allowing for dynamic behavior at a temperature of 350 K. The comparison of bond lengths and angles between AIMD and static DFT reveals good agreement. The results suggest that the dynamic nature of AIMD simulations with a larger number of solvent molecules provides an accurate description of the bond and angle parameters of silicate rings compared to static DFT calculations with micro solvation models.

3.4 Formation of dominant silicate species

The formation of dominant species in the early stages of zeolite formation is known to be dependent on reaction conditions and the presence of counter ions in the solution. For example, in the presence of inorganic cation such as Li^+, the formation of linear and branched silicate is more favorable than the 3-ring structure[25]. On the other hands, the presence of an organic cation such as TEA^+ favors the formation of 3-ring structures over the linear silicate[67]. This study shows that excess hydroxide ion may also play role in controlling the dominant species of silicate formation. The free energy profiles presented in Table 1 imply that in the presence of excess OH^-, the formation of linear tetramer and 4-ring are the most favorable with the lowest overall activation free energy barriers (71 kJ/mol and 73 kJ/mol, respectively). While the rate-limiting step of the silicate growth is the trimerization with the largest activation barrier (102 kJ/mol). This is in contrast to the case without excess hydroxide ion, where the formation of trimer is the most favorable step with a barrier of only 53 kJ/mol (see Table 2). The increase in trimer formation free energy of 49 kJ/mol in the presence of an excess of hydroxide ion could be attributed to an unfavorable interaction due to a higher energy of a doubly charged trimer, relative to a singly charged one. Our findings suggest that silicate growth will be more difficult in a very high pH environment. Because the overall process must overcome the high activation barrier of forming trimer silicate immediately following the first dimerization reaction step. This is consistent with experimental findings that silicate growth was reduced at very high pH values.[35]

A key concept in zeolite synthesis is the formation of a single 3-ring and 4-ring, as well as the formation of D3R and D4R. Depending on the reaction conditions, one structure may form more easily than another. For example, in the presence of organic cation such as TMA^+ or TEA^+, there was a significant difference in the formation of D3R and D4R species.[8,51] An experimental study of Chen et al.[71] has shown that the cation TMA^+ stabilize the D4R structure over the D3R. However, in the case of TEA^+, the a higher stability of the 3-ring/D3R over the 4-ring/D4R was observed[8,72,73]. Analysis of computer simulations[52,69,70] suggests was that the interaction between the organic counter ion and different silicate structures during formation plays a decisive role in the formation of more favorable ring clusters in water solutions. The current study provides evidence for an alternative way to control formation of ring structures in zeolite synthesis by using excess hydroxide. It is worth noting that the mechanism differs from that of the counter ion in that hydroxide ion is reactive and actively participates in the silicate condensation reaction. The overall free energies provided in Table 2 show that

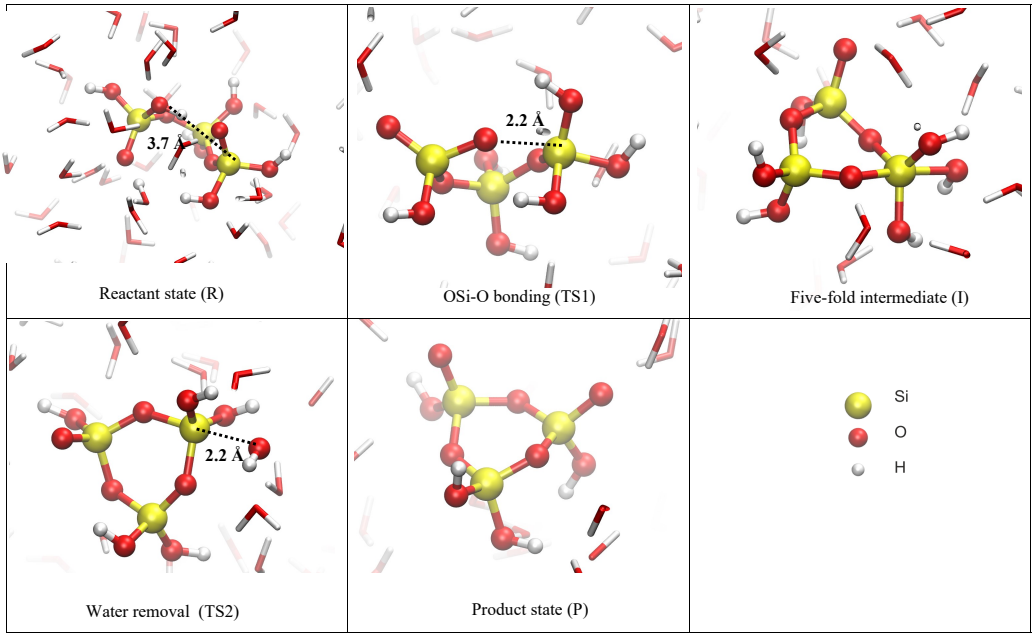

Fig. 6 Representative snapshot from AIMD simulations of the 3-ring formation with the excess of hydroxide ion. Reaction mechanism is described in Scheme 1. For clarity, some water molecules are omitted in the visualization.

in the presence of an excess OH^-, the formation 4-ring is more favorable than the 3-ring structure with the overall free energy barriers of 73 kJ/mol and 92 kJ/mol, respectively. The trend is inverted in the absence of excess hydroxide ion,[24] where the 3-ring structure outperforms the 4-ring. This difference could be due to the unique arrangement of the water surrounding the ring structures observed in previous works.[52,67,70,74].

3.5 The role of excess hydroxide group

The role of pH in zeolite synthesis has been extensively discussed in literature. In the excellent review of Cundy et al.[35], it is stated that the zeolite synthesis is not favorable at acidic environment (pH between 4-7) but more favorable at basic (pH between 8-10). When the pH is above 10, the kinetic of zeolite formation becomes again unfavorable.[35] There was an attempt by Zhang et al.[29] to rationalize this experimental observation with kinetic Monte Carlo simulation of silicate oligomerization. The effect of pH on the rate of formation was modeled using the ratio of $Si(OH)_4$ and $Si(OH)_3^-$ as described in 1. The authors, did not consider the formation of two $Si(OH)_3^-$ and thereby did not account for the effect of excess of an hydroxide group on the mechanismand activation barriers of silicate condensation. However, excess hydroxide appears to induce an almost instant deprotonation of the silicate species, as demonstrated in the previous section. This suggests that in a very high pH environment, excess hydroxide ions may play a significant role in altering the total free energy of silicate and the dominant species in solution. Thus, including this effect in modeling silicate growth appears a crucial aspect, at high pH conditions.

Dupuis et al.[75] showed the role of sodium hydroxide in the dissociation of neutral silicate species using both experiment and computer simulation. According to the study, the hydroxide ion aids neutral silicate dissociation by attacking the Si-O-Si bond. In line with the study by Dupuis et al.[75], our results show an interesting trend of deprotonated silicate dissociation when looking at the backward reaction in Table 1. The findings suggest that when silicate dissociation occurs, the 3-ring and trimer structures are dissolved first. The reason is that trimer and 3-ring structures have the largest free energy level of the product state (45 kJ/mol and 48 kJ/mol, respectively). Thus the backward reaction to dissolve these species would be easier. The branched tetramer, linear trimer, and dimer will then dissociate afterward. The free energy of the product state shows that the 4-ring species (7 kJ/mol) and dimer (16 kJ/mol) are the most stable silicates. Furthermore, the backward activation energy to dissociate 4-ring species is 66 kJ/mol, representing the largest backward barrier. The reverse reaction of 3-ring formation is only 44 kJ/mol. This implies that in the presence of excess hydroxide, the formation of a 3-ring is suppressed. Again, we can see that excess hydroxide plays an important role in the backward silicate dissociation step.

When investigating silicate condensation in an aqueous environment, it is crucial to consider explicit water molecules. Unlike the disordered solid phase of silica[76], prior research has shown that the reactivity of silicate species is not solely determined by the internal hydrogen bond or bonding between silicon and oxygen atoms[24,28,67,68]. Instead, the interaction between silicate and the external hydrogen bonding with the water network plays a crucial role. To illustrate, we plotted the HOMO and LUMO molecular orbital of all six silicate structures in Fig S3 and S4, and compared them with other static DFT calculations[11,14,19]. Although our molecular orbital results are consistent with previous studies, it is important to note that free energy reaction profiles cannot be explained solely based on these features. Additional factors, such as explicit water molecules, must be considered to

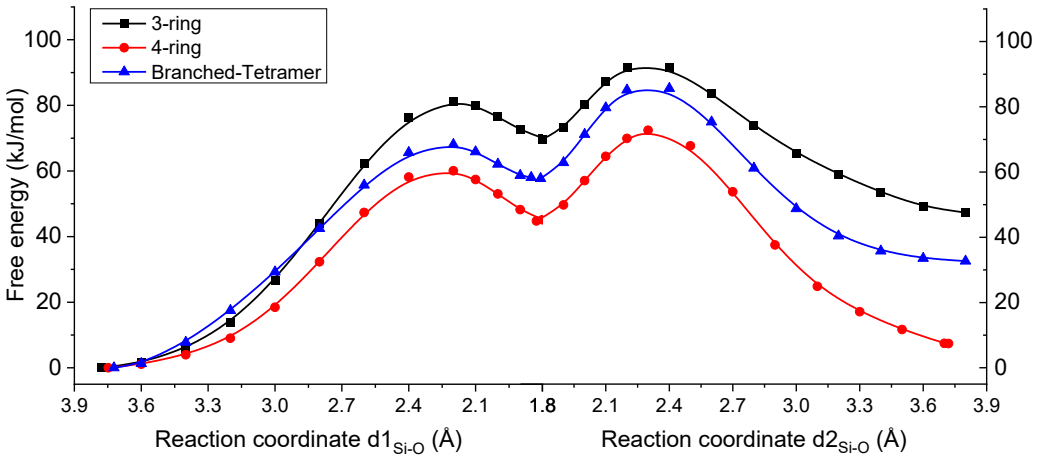

Fig. 7 Calculated free-energy profile (kJ/mol) of formation of ring and branched silicate oligomers as a function of the reaction coordinate. The profiles calculated for the two stages are connected in the graph.

fully understand the silicate condensation process in an aqueous environment.

4 Conclusions

Ab-initio molecular dynamic simulations with a model that incorporates explicit water molecules were used to investigate the formation of silicate oligomers from dimer to 4-ring in the presence of an excess OH^-. The findings indicate that the presence of excess OH^- raises the free energy barriers for the formation of small oligomers. The formation of trimer is the rate-limiting step in silicate growth due to the relatively high free energy barrier. The formation of the linear tetramer appears to have the lowest free energy barrier. The presence of OH^- promotes the formation of a 4-ring rather than a 3-ring. This is consistent with the experimental observation that the rate of silicate oligomer formation is unfavorable at very high pH environment.[35]

The observation that linear trimerization and 3-ring formation have a higher transition state barrier than 4-ring and linear tetramer formation suggests that 4-ring structures predominate in the presence of excess OH^-. Furthermore, the calculated reaction free energies show that 4-ring formation is thermodynamically more stable than 3-ring formation. However, more research is needed to evaluate the free energy profiles of the single- to double-ring formation route in order to evaluate the formation of double rings.

The computational cost of simulating larger silicate systems by AIMD is a currently a major obstacle for systematic studies of the formation of these structures. As such, this work has been limited to the formation of 3-ring and 4-ring structures. To address the double 3-ring and double 4-ring species, alternative approaches such as semi-empirical or ReaxFF methods may be considered in future research.

Finally, our findings shed light on how excess OH^- affects silicate oligomerization by regulating the both thermodynamic and kinetic parameters of reactions. By actively participating in the condensation reaction and modifying hydrogen bonding in the solvation shell, OH^- promotes the formation of larger oligomers. This study clearly shows that the role of pH in zeolite synthesis is not only to control the ratio of neutral and negatively charged silicate species, but also to significantly alter the reaction rate of silicate oligomerization. This is a necessary input for larger scale simulations such as kinetic Monte Carlo to provide a bigger picture of zeolite synthesis to match with experimental scale.

Conflicts of interest

There are no conflicts to declare.

Acknowledgements

This work was carried out on the Dutch national e-infrastructure with the support of SURF Cooperative.

Notes and references

1 C. J. Brinker and G. W. Scherer, *Sol-Gel Science*, Elsevier, 1990.
2 P. Bussian, F. Sobott, B. Brutschy, W. Schrader and F. Schüth, *Angew. Chem. Int. Ed.*, 2000, **39**, 3901–3905.
3 N. Danilina, F. Krumeich, S. A. Castelanelli and J. A. van Bokhoven, *J. Phys. Chem. C*, 2010, **114**, 6640–6645.
4 J. Dědeček, S. Sklenak, C. Li, B. Wichterlová, V. Gábová, J. Brus, M. Sierka and J. Sauer, *J. Phys. Chem. C*, 2009, **113**, 1447–1458.
5 A. Depla, D. Lesthaeghe, T. S. van Erp, A. Aerts, K. Houthoofd, F. Fan, C. Li, V. Van Speybroeck, M. Waroquier, C. E. Kirschhock and J. A. Martens, *J. Phys. Chem. C*, 2011, **115**, 3562–3571.
6 J. M. Fedeyko, H. Egolf-Fox, D. W. Fickel, D. G. Vlachos and R. F. Lobo, *Langmuir*, 2007, **23**, 4532–4540.
7 G. J. McIntosh, P. J. Swedlund and T. Söhnel, *Phys. Chem. Chem. Phys.*, 2011, **13**, 2314–2322.
8 S. A. Pelster, B. Weimann, B. B. Schaack, W. Schrader and F. Schüth, *Angew. Chem. Int. Ed.*, 2007, **46**, 6674–6677.
9 S. Sklenak, J. Dědeček, C. Li, B. Wichterlová, V. Gábová,

M. Sierka and J. Sauer, *Angew. Chem. Int. Ed.*, 2007, **46**, 7286–7289.
10 J. A. van Bokhoven, T.-L. Lee, M. Drakopoulos, C. Lamberti, S. Thieß and J. Zegenhagen, *Nature Mater*, 2008, **7**, 551–555.
11 T. T. Trinh, A. P. Jansen and R. A. van Santen, *J. Phys. Chem. B*, 2006, **110**, 23099–23106.
12 R. van Santen and J. Niemantsverdriet, *Chemical Kinetics and Catalysis*, Springer US, 1995.
13 J. R. Gomes, M. N. D. Cordeiro and M. Jorge, *Geochim. Cosmochim. Acta*, 2008, **72**, 4421–4439.
14 H. Henschel, A. M. Schneider and M. H. Prosenc, *Chem. Mater.*, 2010, **22**, 5105–5111.
15 G.-F. Jiao, M. Pu and B.-H. Chen, *Struct Chem*, 2008, **19**, 481–487.
16 X. Liu, X. Lu, E. J. Meijer, R. Wang and H. Zhou, *Geochim. Cosmochim. Acta*, 2010, **74**, 510–516.
17 M. J. Mora-Fonz, C. R. A. Catlow and D. W. Lewis, *Angew. Chem. Int. Ed.*, 2005, **44**, 3082–3086.
18 M. J. Mora-Fonz, C. R. A. Catlow and D. W. Lewis, *J. Phys. Chem. C*, 2007, **111**, 18155–18158.
19 C. L. Schaffer and K. T. Thomson, *J. Phys. Chem. C*, 2008, **112**, 12653–12662.
20 C.-S. Yang, J. M. Mora-Fonz and C. R. A. Catlow, *J. Phys. Chem. C*, 2012, **116**, 22121–22128.
21 B. Szyja, P. Vassilev, T. Trinh, R. van Santen and E. Hensen, *Microporous Mesoporous Mater.*, 2011, **146**, 82–87.
22 Y. Li and J. Yu, *Chem. Rev.*, 2014, **114**, 7268–7316.
23 M. Ciantar, C. Mellot-Draznieks and C. Nieto-Draghi, *J. Phys. Chem. C*, 2015, **119**, 28871–28884.
24 T. T. Trinh, A. P. Jansen, R. A. van Santen and E. J. Meijer, *J. Phys. Chem. C*, 2009, **113**, 2647–2652.
25 T. T. Trinh, A. P. Jansen, R. A. van Santen, J. VandeVondele and E. J. Meijer, *ChemPhysChem*, 2009, **10**, 1775–1782.
26 C. E. White, J. L. Provis, G. J. Kearley, D. P. Riley and J. S. van Deventer, *Dalton Trans.*, 2011, **40**, 1348–1355.
27 T. T. Trinh, A. P. Jansen, R. A. van Santen and E. Jan Meijer, *Phys. Chem. Chem. Phys.*, 2009, **11**, 5092.
28 A. Pavlova, T. T. Trinh, R. A. van Santen and E. J. Meijer, *Phys. Chem. Chem. Phys.*, 2013, **15**, 1123–1129.
29 X.-Q. Zhang, T. T. Trinh, R. A. van Santen and A. P. Jansen, *J. Am. Chem. Soc.*, 2011, **133**, 6613–6625.
30 T. T. Trinh, X. Rozanska, F. Delbecq and P. Sautet, *Phys. Chem. Chem. Phys.*, 2012, **14**, 3369.
31 X.-Q. Zhang, T. T. Trinh, R. A. van Santen and A. P. Jansen, *J. Phys. Chem. C*, 2011, **115**, 9561–9567.
32 H. Xia, X. Fan, J. Zhang, H. He and Q. Guo, *J. Phys. Chem. A*, 2021, **125**, 8827–8835.
33 M. Ciantar, T. T. Trinh, C. Michel, P. Sautet, C. Mellot-Draznieks and C. Nieto-Draghi, *Angew. Chem.*, 2021, **133**, 7187–7192.
34 J. E. Schmidt, D. Fu, M. W. Deem and B. M. Weckhuysen, *Angew. Chem. Int. Ed.*, 2016, **55**, 16044–16048.
35 C. S. Cundy and P. A. Cox, *ChemInform*, 2003, **34**, 663–702.
36 D. Tleugabulova, A. M. Duft, Z. Zhang, Y. Chen, M. A. Brook and J. D. Brennan, *Langmuir*, 2004, **20**, 5924–5932.
37 H.-P. Lin and C.-Y. Mou, *Acc. Chem. Res.*, 2002, **35**, 927–935.
38 R. M. Smith and A. E. Martell, *Critical Stability Constants*, Springer US, 1975, vol. 1.
39 F. Gruy, M. Kamińska and J. Valente, *Colloids Surf., A*, 2021, **628**, 127238.
40 S. Biswas, H. Kwon, K. C. Barsanti, N. Myllys, J. N. Smith and B. M. Wong, *Phys. Chem. Chem. Phys.*, 2020, **22**, 26265–26277.
41 S. Biswas and B. M. Wong, *J. Mol. Liq.*, 2021, **330**, 115624.
42 J. Hutter, M. Iannuzzi, F. Schiffmann and J. VandeVondele, *WIREs Comput Mol Sci*, 2013, **4**, 15–25.
43 J. VandeVondele, M. Krack, F. Mohamed, M. Parrinello, T. Chassaing and J. Hutter, *Comput. Phys. Commun.*, 2005, **167**, 103–128.
44 S. Goedecker, M. Teter and J. Hutter, *Phys. Rev. B*, 1996, **54**, 1703–1710.
45 C. Hartwigsen, S. Goedecker and J. Hutter, *Phys. Rev. B*, 1998, **58**, 3641–3662.
46 A. Becke, *Phys. Rev. A*, 1988, **38**, 3098–3100.
47 C. Lee, W. Yang and R. G. Parr, *Phys. Rev. B*, 1988, **37**, 785–789.
48 S. Grimme, *J. Comput. Chem.*, 2006, **27**, 1787–1799.
49 J. VandeVondele and J. Hutter, *The Journal of Chemical Physics*, 2007, **127**, 114105.
50 G. Bussi, D. Donadio and M. Parrinello, *The Journal of Chemical Physics*, 2007, **126**, 014101.
51 B. B. Schaack, W. Schrader and F. Schüth, *Angew. Chem. Int. Ed.*, 2008, **47**, 9092–9095.
52 T. T. Trinh, K.-Q. Tran, X.-Q. Zhang, R. A. van Santen and E. J. Meijer, *Phys. Chem. Chem. Phys.*, 2015, **17**, 21810–21818.
53 E. Carter, G. Ciccotti, J. T. Hynes and R. Kapral, *Chem. Phys. Lett.*, 1989, **156**, 472–477.
54 M. Sprik and G. Ciccotti, *The Journal of Chemical Physics*, 1998, **109**, 7737–7744.
55 T. S. van Erp and E. J. Meijer, *Angew. Chem. Int. Ed.*, 2004, **43**, 1660–1662.
56 I. Ivanov and M. L. Klein, *J. Am. Chem. Soc.*, 2002, **124**, 13380–13381.
57 J.-W. Handgraaf and E. J. Meijer, *J. Am. Chem. Soc.*, 2007, **129**, 3099–3103.
58 N. Govindarajan, A. Tiwari, B. Ensing and E. J. Meijer, *Inorg. Chem.*, 2018, **57**, 13063–13066.
59 F. Saiz and L. Bernasconi, *Catal. Sci. Technol.*, 2021, **11**, 4560–4569.
60 J. Schmidt, J. VandeVondele, I.-F. W. Kuo, D. Sebastiani, J. I. Siepmann, J. Hutter and C. J. Mundy, *J. Phys. Chem. B*, 2009, **113**, 11959–11964.
61 M. Sprik, J. Hutter and M. Parrinello, *The Journal of Chemical Physics*, 1996, **105**, 1142–1152.
62 T. Todorova, A. P. Seitsonen, J. Hutter, I.-F. W. Kuo and C. J. Mundy, *J. Phys. Chem. B*, 2005, **110**, 3685–3691.
63 M. Chen, H.-Y. Ko, R. C. Remsing, M. F. Calegari Andrade,

B. Santra, Z. Sun, A. Selloni, R. Car, M. L. Klein, J. P. Perdew and X. Wu, *Proc. Natl. Acad. Sci. U.S.A.*, 2017, **114**, 10846–10851.

64 G. Hura, J. M. Sorenson, R. M. Glaeser and T. Head-Gordon, *The Journal of Chemical Physics*, 2000, **113**, 9140–9148.

65 A. Soper and C. Benmore, *Phys. Rev. Lett.*, 2008, **101**, 065502.

66 L. B. Skinner, C. Huang, D. Schlesinger, L. G. Pettersson, A. Nilsson and C. J. Benmore, *The Journal of Chemical Physics*, 2013, **138**, 074506.

67 N. L. Mai, H. T. Do, N. H. Hoang, A. H. Nguyen, K.-Q. Tran, E. J. Meijer and T. T. Trinh, *J. Phys. Chem. B*, 2020, **124**, 10210–10218.

68 M. Moqadam, E. Riccardi, T. T. Trinh, A. Lervik and T. S. van Erp, *Phys. Chem. Chem. Phys.*, 2017, **19**, 13361–13371.

69 S. Caratzoulas, D. G. Vlachos and M. Tsapatsis, *J. Am. Chem. Soc.*, 2005, **128**, 596–606.

70 S. Caratzoulas and D. Vlachos, *J. Phys. Chem. B*, **112**, 7–10.

71 Y. Chen, N. M. Washton, R. P. Young, A. J. Karkamkar, J. J. De Yoreo and K. T. Mueller, *Phys. Chem. Chem. Phys.*, 2019, **21**, 4717–4720.

72 S. A. Pelster, R. Kalamajka, W. Schrader and F. Schüth, *Angew. Chem. Int. Ed.*, 2007, **46**, 2299–2302.

73 S. Inagaki, K. Nakatsuyama, Y. Saka, E. Kikuchi, S. Kohara and M. Matsukata, *J. Phys. Chem. C*, 2007, **111**, 10285–10293.

74 S. Caratzoulas, D. Vlachos and M. Tsapatsis, *J. Phys. Chem. B*, 2005, **109**, 10429–10434.

75 R. Dupuis, R. Pellenq, J.-B. Champenois and A. Poulesquen, *J. Phys. Chem. C*, 2020, **124**, 8288–8294.

76 F. Saiz and N. Quirke, *Phys. Chem. Chem. Phys.*, 2018, **20**, 27528–27538.